A unified framework for robust stability analysis of linear irrational systems in the parametric space

Rachid Malti, Milan Rapaic, Vukan Turkulov

A unified framework for robust stability analysis of linear irrational systems in the parametric space ⋆

Rachid Malti [a], Milan R. Rapaic [b], Vukan Turkulov [b]

[a] *Univ. Bordeaux, IMS – UMR 5218 CNRS, France*

[b] *Faculty of Technical Sciences, Trg Dositeja Obradovića 6, University of Novi Sad, Serbia*

Abstract

This paper presents a unified framework for robust stability analysis of linear stationary systems with irrational transfer functions in the space of an arbitrary number of unknown parameters. Systems of this kind are encountered when analyzing distributed parameter systems, time delayed systems of both retarded and neutral type, or even fractional systems. Systems described by irrational transfer functions are of infinite dimension, typically having an infinite number of poles and/or zeros, rendering their stability analysis more challenging as compared to their finite-dimensional counterparts. First, it is proven that, under mild hypotheses, new poles with positive real parts may appear through a continuous variation of parameters only if existing stable poles cross the imaginary axis. Hence, by determining parametric values for which the crossing occurs, known as stability crossing sets (SCS), the entire parametric space is separated into regions within which the number of right-half poles (including their multiplicity) is invariant. Based on the aforementioned result, a robust estimation algorithm, formulated as an interval constraint satisfaction problem, is solved using guaranteed methods, for determining the SCS. The developed algorithm is applied for assessing stability of (i) a controlled parabolic 1D partial differential equation, namely the heat equation, in finite and semi-infinite media, (ii) time-delay rational systems with distributed and retarded type delays, (iii) fractional systems, providing stability results even for incommensurate differentiation orders.

Key words: Stability; Time-delay systems; Distributed parameter systems; Interval arithmetics; Guaranteed stability.

1 Introduction

Many engineering systems exhibit dynamical behaviors that can be captured by partial differential equations (PDE), or delayed ordinary (and partial) differential equations. These distributed parameter systems (DPS) yield irrational transfer functions that are usually infinite dimensional, with an infinite number of poles and/or zeros. A wide variety of transfer functions of DPS, solutions of PDE, is exhibited in Curtain & Morris (2009).

This paper presents stability analysis of irrational transfer functions in the parametric space. Similar methods have been investigated for stability analysis of time-delay-systems (TDS) in Gryazina (2004); Neimark (1998); Lee & Hsu (1969); El'sgol'ts & Norkin (1973). They split the parametric space into multiple regions, with the number of unstable poles being invariant inside each region. An alternative approach consists of finding the stability crossing sets (SCS), i.e. a set of surfaces for which there is at least a pole crossing the imaginary axis. Such approaches have been successfully demonstrated for retarded systems with two and three independent delays Hale & Huang (1993); Gu, Niculescu & Chen (2005); Sipahi & Olgac (2005); Gu & Naghnaeian (2011), providing insightful graphical representation of stability equivalence regions. To the best of authors' knowledge, such methods have never been extended to other types of irrational transfer functions.

A new method, based on the application of Rouché's theorem in the frequency domain, has recently been proposed for stability analysis of fractional systems in Rapaić & Malti (2019) and a large class of retarded and distributed TDS in Turkulov, Rapaić & Malti (2022). Given a parametrized fractional and/or TDS and an arbitrary parametric point, the proposed method identifies the surrounding region in the parametric space for which the number of unstable poles remains invariant.

⋆ This paper was not presented at any IFAC meeting. Corresponding author R. Malti

Email addresses: rachid.malti@ims-bordeaux.fr (Rachid Malti), rapaja@uns.ac.rs (Milan R. Rapaic), vukan_turkulov@uns.ac.rs (Vukan Turkulov).

Another important tool has been continuously used for stability analysis of irrational transfer functions: the Nyquist stability criterion. It has been used for analyzing stability of (i) DPS in Chait, MacCluer & Radcliffe (1989); Logemann (1991), (ii) time-delay (retarded-type) fractional transfer functions in Zhang, Liu & Xue (2020), and (iii) incommensurate fractional transfer functions in Ivanova, Moreau & Malti (2016). Some other well-known finite-dimensional results, such as circle criterion and small gain theorem, have been generalized to a large class of DPS in Logemann (1991).

Another category of methods is based on the state-space representation and some special forms of Lyapunov–Krasovskii functionals. It is used to derive simple finite dimensional conditions in terms of LMI's for assessing stability of distributed parameter systems with time delays in Fridman & Orlov (2009), and of uncertain fractional order systems of neutral type with distributed delays in Aghayan, Alfi & Machado (2021). Additionally, direct Lyapunov method is used in Katz & Fridman (2020) for stability of a finite dimensional observer based control of a 1-D parabolic PDE (linear heat equation). Moreover, in Katz & Fridman (2021), robustness of such finite-dimensional controllers is studied with respect to input and output delays. Furthermore, Prieur & Trélat (2019) synthesize stabilizing boundary control subject to a constant delay for a reaction-diffusion partial differential equation by stabilizing unstable poles of the infinite dimensional system.

Several methods are developed for analyzing stability of important specific DPS such as clamped-free damped string Lhachemi, Saussié, Zhu & Shorten (2020), telegrapher's equation Sano (2018), heat equation Li, Zhou & Gao (2018); Li & Gao (2021), wave equation Gao, Ma & Sun (2019); Ha-Duong & Joly (1994).

A unified framework is proposed in this paper for stability analysis of linear irrational and/or DPS in the frequency domain. The proposed method is based on computing the SCS of a wide range of systems that include (i) solutions of some partial differential equations, with or without delays, under some boundary conditions, which transfer functions may include terms like $e^{-\sqrt{s}}$, $\cosh(\sqrt{s})$, or $\sinh(\sqrt{s})$, of the Laplace variable s, (ii) TDS with retarded, incommensurate or distributed delays, (iii) fractional systems, with or without time-delays, which may have incommensurate differentiation orders and which stability analysis is more challenging than the commensurate ones.

The paper is organized as follows. Notation and hypotheses are presented in section 1.2 followed by the problem formulation. Then, theoretical results regarding pole continuity are presented in section 2, followed by a robust estimation algorithm of the SCS, based on interval arithmetics, in section 3. Applications to DPS, TDS and fractional systems are presented in sections 4, 5, and 6 respectively, before concluding.

1.1 Notation

The paper utilizes standard mathematical notations. The set of non-negative and non-positive real numbers are respectively denoted by $\mathbb{R}^+$ and $\mathbb{R}^-$. $\mathbb{C}$ is the field of complex numbers, $\mathbb{C}^+$ the open right-half complex plane $\{s \in \mathbb{C} : \mathscr{Re}(s) > 0\}$, and $\overline{\mathbb{C}^+}$ the closed right-half complex plane $\{s \in \mathbb{C} : \mathscr{Re}(s) \geq 0\}$.

When dealing with linear time-invariant (LTI) rational systems, the concept of a characteristic function (polynomial) is well defined as transfer function denominator. It allows assessing system stability by examining the zeros of the characteristic function.

However, when dealing with LTI, irrational, possibly infinite dimensional, systems denoted $G(s, \boldsymbol{\theta})$, where $s \in \mathbb{C}$ is the Laplace variable, and $\boldsymbol{\theta} = (\theta_1, \cdots, \theta_n) \in \mathcal{T} \subset \mathbb{R}^n$, is the parametric vector, the concept of characteristic function $f(s, \boldsymbol{\theta})$ requires some clarifications:

(1) f has no finite poles of any multiplicity,
(2) f has branching points and/or essential singularities everywhere G has branching points and/or essential singularities,
(3) all finite zeros of f match poles of G in both location and multiplicity.

The selection of the characteristic function is not unique. Several different characteristic functions may be constructed from a single transfer function, according to the points above. For example, a characteristic function of a given transfer function $G(s, \boldsymbol{\theta})$ could be derived as

$$f(s, \boldsymbol{\theta}) = \frac{Q(s, \boldsymbol{\theta})}{G(s, \boldsymbol{\theta})} , \tag{1}$$

with Q being an arbitrary analytic function in $\mathbb{C}$ having zeros at the same locations with matching multiplicities as G.

Additionally, let Ω_f denote the *stability crossing set* (SCS) of f, i.e. a set of surfaces for which there is at least a zero of f crossing the imaginary axis

$$\Omega_f = \{\boldsymbol{\theta} \in \mathcal{T} \,|\, f(\mathrm{j}\omega, \boldsymbol{\theta}) = 0 \text{ for some } \omega \in \mathbb{R}\} . \tag{2}$$

Let $NU_f(\boldsymbol{\theta})$ denote the number of zeros of a characteristic function $f(s, \boldsymbol{\theta})$ with a non-negative real part, where each zero is counted as many times as its multiplicity.

1.2 Problem formulation

Consider an LTI system with characteristic equation $f(s,\boldsymbol{\theta})$, $\boldsymbol{\theta} \in \mathcal{T} \subset \mathbb{R}^n$. The problem under consideration can be formulated as partitioning the parametric space into regions $\mathcal{T}_k$ $(k \in 1,\ldots,K)$ such that for all k

i) $f(s,\boldsymbol{\theta})$ has no zero on the imaginary axis, for all $\boldsymbol{\theta} \in \mathcal{T}_k$, and
ii) $NU_f(\boldsymbol{\theta}_1) = NU_f(\boldsymbol{\theta}_2)$ for all $\boldsymbol{\theta}_1, \boldsymbol{\theta}_2 \in \mathcal{T}_k$.

The solution will be sought under the following hypotheses on f and $\mathcal{T}$:

(H1) For every $\boldsymbol{\theta} \in \mathcal{T}$, $s \mapsto f(s,\boldsymbol{\theta})$ is analytic in $\overline{\mathbb{C}^+}$ [1], except possibly in a finite set of points $s = \mathrm{j}\omega$ with $\omega \in \Xi = \{\omega_1,\ldots,\omega_N\}$. For every $s \in \overline{\mathbb{C}^+} \setminus \mathrm{j}\Xi$, $\boldsymbol{\theta} \mapsto f(s,\boldsymbol{\theta})$ is continuous on $\mathcal{T}$.
(H2) For all $\omega_k \in \Xi$, there exist $\epsilon_k > 0$ such that $f(s,\boldsymbol{\theta}) \neq 0$ for all s satisfying $\mathscr{Re}(s) \geq 0$ and $|s - \mathrm{j}\omega| \leq \epsilon_k$, and all $\boldsymbol{\theta} \in \mathcal{T}$.
(H3) There exists $M > 0$ such that $f(s,\boldsymbol{\theta}) \neq 0$ for every $\boldsymbol{\theta} \in \mathcal{T}$ and all s such that $\mathscr{Re}(s) \geq 0$ and $|s| \geq M$.

According to (H1), $f(s,\boldsymbol{\theta})$ must be continuous with respect to $\boldsymbol{\theta}$ and analytic with respect to $s \in \overline{\mathbb{C}^+}$, except possibly at a finite number of points on the imaginary axis. Those singular points are collected within a set $\mathrm{j}\Xi$ and illustrated by red dots in Fig.1. Hypotheses (H2) and (H3) restrict admissible locations of the right-half zeros. According to (H2), roots of $f(s,\boldsymbol{\theta})$ cannot stem from any singular point belonging to the set $\mathrm{j}\Xi$ for any value of $\boldsymbol{\theta}$. According to (H3), roots of $f(s,\boldsymbol{\theta})$ cannot have arbitrary large positive real parts.

Even though the introduced hypotheses limit the set of admissible characteristic functions, they are not very restrictive. Hypothesis (H1), in particular, excludes systems having branching points and/or essential singularities with positive real parts. Such systems are exponentially unstable, so that investigation of the location of their characteristic function roots loses all practical significance. To clarify, consider a characteristic function having such a singularity at $s = 1$. By construction, this characteristic function has to be obtained from a transfer function having a singularity at $s = 1$, implying that its abscissa of convergence is at least equal to 1, and consequently that its impulse response grows asymptotically at least as fast as e^t. As an example, consider a transfer

[1] A function is analytic in a closed set if and only if it is analytic at every point of that set. For sets having nonempty boundary (like $\overline{\mathbb{C}^+}$) this actually means that the function is also analytic in some (possibly small) neighborhood of that boundary. In other words, a function analytic in a closed set is also analytic in some open superset that encloses that set.

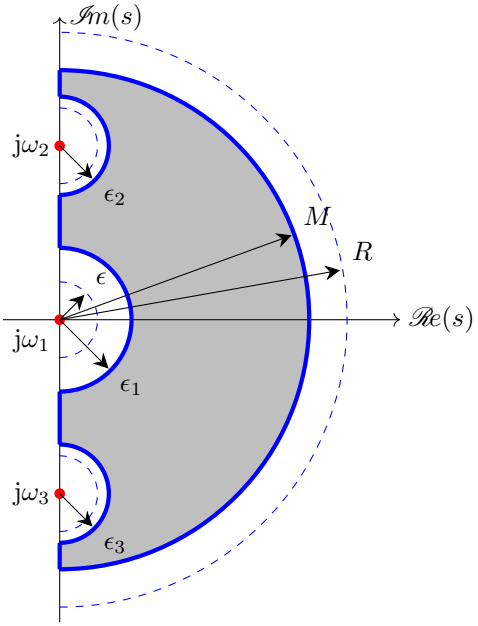

Fig. 1. Illustration of the notation involved in the hypotheses (H1)-(H3) and in the proof of Theorem 2.

function $G(s) = \frac{\sqrt{s-1}}{s+1}$, which impulse response is

$$\mathcal{L}^{-1}\{G(s)\} = \frac{e^t}{\sqrt{\pi t}} - \sqrt{2}\mathrm{Erfi}(\sqrt{2t})e^{-t}\,,$$

where Erfi is the "imaginary error function" ($\mathrm{Erfi}(z) = -\mathrm{jErf}(\mathrm{j}z)$, with Erf being the common "error function"). A corresponding characteristic function could be constructed by choosing $Q(s) = 1$ in (1), $f(s) = \frac{s+1}{\sqrt{s-1}}$. Hence, if f is not analytic in $\overline{\mathbb{C}^+} \setminus \mathrm{j}\Xi$, as suggested in (H1), the location of its zeros is not sufficient to assess system stability.

The introduced hypotheses also limit the extent of the parametric space $\mathcal{T}$. Hypothesis (H2) is a safeguard from cases in which right-half zeros of the characteristic function either originate from or terminate at the singularities located on the imaginary axis. A simple example would be a system with characteristic function $f(s,K) = K + s^{-\frac{3}{2}}$, having a zero with positive real part originating from the origin when $K < 0$. This however is not permitted by (H2) which hence restricts the study of $f(s,K)$ to $K > 0$. Hypothesis (H3) guards against cases in which zeros emerge from infinity in $\mathbb{C}^+$. It, for example, prevents negative values of delays (non-causal leads), and also safeguards against cases in which system structure abruptly changes for certain parametric values. An interesting practical example is the case of loop transfer function with relative degree zero, such as e.g. $L(s,K) = K\frac{1-s}{s+1}$. Its closed-loop characteristic polynomial is $f(s,K) = (s+1) + K(s-1)$. In this particular case, a single branch of the root locus originates at $s = -1$ for $K = 0$. By increasing K the root slides along

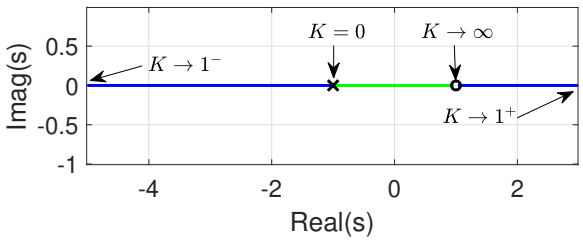

Fig. 2. Root locus of closed loop system with loop transfer function $L(s, K) = K\frac{1-s}{1+s}$.

the negative real axis, and reaches asymptotically $-\infty$ when $K \to 1^-$, as illustrated in Fig.2 . The value $K = 1$ is singular, since the order of the system changes, and for this particular value of K the characteristic polynomial has no zero. However when $K > 1$, a root pops up from $+\infty$, and decreases asymptotically to $s = 1$ as K grows. Consequently, the characteristic function of this system does not fulfill hypothesis $(H3)$ when $K \in \mathbb{R}$. However, it is worth mentioning that $(H3)$ allows investigating separately the stability for $1 < K \leq K_{\max} < \infty$.

Within the present work and under hypothesis (H1)-(H3), we start by proving that the only way for the number of zeros of a characteristic function to change, when the parameters vary continuously, is by crossing the imaginary axis. This theoretical result, related to root continuity, is studied in section 2. Then, a new and robust estimation algorithm, is detailed in section 3 for computing the SCS for this large class of systems. Unlike many previously published results, mainly focused on time-delay systems (TDS) Gu et al. (2005); Sipahi & Delice (2009); Morărescu, Niculescu & Gu (2007), a unified approach is proposed in the present paper that applies to a large variety of irrational systems, regardless of the number of investigated parameters. The only practical limitation is related to the exponential complexity of the proposed algorithm.

2 Root Continuity

The following claims will ensure continuity of all right-half zeros of the characteristic function. Start by recalling the root continuity result from (Dieudonné, 1960, Theorem 9.17.4).

Theorem 1 *Let D be an open set in $\mathbb{C}$, $\mathcal{T}$ a metric space, F a continuous, complex valued function in $\mathbb{C} \times \mathcal{T}$ such that for each $\boldsymbol{\theta} \in \mathcal{T}$ $s \mapsto f(s, \theta)$ is analytic in D. Let D_1 be an open subset of D whose closure $\overline{D_1}$ is compact and contained in D, and let $\boldsymbol{\theta}_0$ be such that no zero of $f(s, \boldsymbol{\theta}_0)$ is on the boundary of D_1. Then, there exists a neigborhood W of $\boldsymbol{\theta}_0$ such that for every $\boldsymbol{\theta} \in W$*

(1) there are no zeros of $f(s, \boldsymbol{\theta})$ on the boundary of D_1, and

(2) the sum of the orders of zeros of $f(s, \boldsymbol{\theta})$ belonging to D_1 is independent of $\boldsymbol{\theta}$.

All the pre-requisites are met now, for the main result of the paper to be stated and proven.

Theorem 2 *Under hypotheses (H1)-(H3), given any connected subset $\mathcal{S}$ of $\mathcal{T}$, if $f(\mathrm{j}\omega, \boldsymbol{\theta}) \neq 0$ for all $\omega \in \mathbb{R} \setminus \Xi$ and all $\boldsymbol{\theta} \in \mathcal{S}$, then for any $\boldsymbol{\theta}_1, \boldsymbol{\theta}_2 \in \mathcal{S}$ the number of zeros of f in $\overline{\mathbb{C}^+}$, counting their multiplicities, is the same: $NU_f(\boldsymbol{\theta}_1) = NU_f(\boldsymbol{\theta}_2)$.*

PROOF. According to (H1), there exists an open set D containing $\overline{\mathbb{C}^+} \setminus \mathrm{j}\Xi$ such that f is continuous on $D \times \mathcal{T}$. Let M satisfy (H3), and select an arbitrary $R \geq \max\{M, |\omega_1|, \ldots, |\omega_N|\}$, with $\omega_k \in \Xi$. Consider ϵ_k, introduced in (H2), and define $0 < \epsilon \leq \min_k \epsilon_k$. Introduce set $\overline{D_1}$ as the closed set bounded by the imaginary axis excluding $\mathrm{j}[\omega_k - \epsilon, \omega_k + \epsilon]$, "small" semi-circles $\mathrm{j}\omega + \epsilon^{\mathrm{j}\varphi}$ and the "big" semi-circle $Re^{\mathrm{j}\varphi}$ (with $\varphi \in [-\frac{\pi}{2}, \frac{\pi}{2}]$). Let D_1 be the interior of $\overline{D_1}$. Due to hypotheses (H2), (H3), and the condition $f(\mathrm{j}\omega, \boldsymbol{\theta}) \neq 0$ imposed in the theorem, there can be no zeros of f on the boundary of D_1 for all $\boldsymbol{\theta} \in \mathcal{S}$. Therefore, D_1 satisfies all the assumptions of Theorem 1. Consequently, for all $\boldsymbol{\theta_0} \in \mathcal{S}$ there exists a neighborhood $W(\boldsymbol{\theta}_0) \subset \mathcal{S}$ such that the number of zeros of f inside D_1, including multiplicities, is independent of $\boldsymbol{\theta} \in W(\boldsymbol{\theta_0})$. Notice further that this implies that the number of zeros (including multiplicities) of f is constant within $\overline{\mathbb{C}^+}$, since due to (H2) there can be no right-half singularities within the "small" semicircles of D_1, and due to (H3) there can be no right-half roots with modulus greater than $M < R$. Consequently, for every $\boldsymbol{\theta_0} \in \mathcal{S}$ there exists a neighborhood $W(\boldsymbol{\theta_0})$ such that the number of zeros in $\overline{\mathbb{C}^+}$ is independent of $\boldsymbol{\theta} \in W(\boldsymbol{\theta_0})$. In the remainder, it is proven by contradiction that the number of right-half zeros of f, including multiplicities, does not change within the entire set $\mathcal{S}$. *Assume that the number of roots, counting multiplicities, is not the same for every $\boldsymbol{\theta} \in \mathcal{S}$.* Then, there exists at least two parametric points $\boldsymbol{\theta}_1$, $\boldsymbol{\theta}_2 \in \mathcal{S}$ such that the number of zeros at $\boldsymbol{\theta}_1$ is different from the one at $\boldsymbol{\theta}_2$. Since $\mathcal{S}$ is connected by assumption, there exists a simple path $\mathcal{P} \subset \mathcal{S}$ connecting $\boldsymbol{\theta}_1$ and $\boldsymbol{\theta}_2$, and at least one point $\boldsymbol{\theta}_0 \in \mathcal{P}$ such that the number of zeros, counting multiplicities, is not constant in any neighborhood of $\boldsymbol{\theta}_0$, which contradicts the existence of $W(\boldsymbol{\theta_0})$ and completes the proof. □

Definition 3 *Given a parametric space $\mathcal{T}$, and an LTI system with characteristic function $f(s, \boldsymbol{\theta})$ with stability crossing set Ω_f, defined in (2), any two points $\boldsymbol{\theta}_1$ and $\boldsymbol{\theta}_2$ from $\mathcal{T}$ are said to belong to the same* ***parametric region*** *if there exists a continuous path within $\mathcal{T}$ connecting $\boldsymbol{\theta}_1$ with $\boldsymbol{\theta}_2$ which does not intersect Ω_f.*

Notice that *"belong to the same parametric region"* is an equivalence relation. Therefore, the stability crossing

set splits the parametric space $\mathcal{T}$ into multiple disjoint regions $\mathcal{T}_k$, $k = 1, \ldots, K \leq \infty$ such that

$$\mathcal{T} = \Omega_f \cup \bigcup_{k=1,\ldots K} \mathcal{T}_k \, .$$

Corollary 4 *Given any parametric region $\mathcal{T}_k$ of $\mathcal{T}$, and any pair of points $\boldsymbol{\theta}_1, \boldsymbol{\theta}_2 \in \mathcal{T}_k$, the number of zeros in $\overline{\mathbb{C}^+}$, counting multiplicities, is the same for $f(s, \boldsymbol{\theta}_1)$ and $f(s, \boldsymbol{\theta}_2)$.*

PROOF. The corollary follows directly from Theorem 2, by noticing that $\mathcal{T}_k$ satisfies all conditions imposed on $\mathcal{S}$. □

Theorem 2 and corollary 4 suggest, under hypotheses (H1)-(H3), that characteristic function zeros (system poles) cannot suddenly appear or change multiplicity in the right-half complex plane. The only way for the number of right-half zeros to change is by crossing the imaginary axis when system parameters change. Hence, the determination of the SCS, defined in (2), allows characterizing all the regions in the parametric space inside which the characteristic function has the same number of zeros.

Theorem 1 was previously used in Cooke & Grossman (1982); Gu et al. (2005) for stability analysis of TDS, by investigating the SCS. Theorem 2 extends these results to arbitrary LTI systems, as long as their characteristic functions satisfy hypotheses (H1)-(H3).

The required theoretical results for root continuity being established, a new and robust estimation algorithm is developed in the next section for determining the SCS.

3 Robust estimation algorithm of the SCS

Since the parameters gathered in $\boldsymbol{\theta}$ vary continuously, the problem of determining stability regions can be reformulated as finding the SCS, defined in (2), for which the zeros of $f(s, \boldsymbol{\theta})$ cross the imaginary axis, i.e. for which

$$\mathcal{CSP}: \begin{cases} \mathscr{R}e\{f(\mathrm{j}\omega, \boldsymbol{\theta})\} = 0 \\ \mathscr{I}m\{f(\mathrm{j}\omega, \boldsymbol{\theta})\} = 0 \\ (\omega, \boldsymbol{\theta}) \in \{\mathbb{R}^+ \setminus \Xi\} \times \mathcal{T} \end{cases} \tag{3}$$

The searching space is restricted to the positive real axis, because all real-valued impulse-response systems have complex conjugate poles. If complex poles do not come in conjugate pairs, then the searching domain is $\{\mathbb{R} \setminus \Xi\}$.

Equation (3) is formulated as a constraint satisfaction problem which solution set of all the feasible parameters is rewritten as

$$\mathbb{S} = \Big\{ (\omega, \boldsymbol{\theta}) \in \{\mathbb{R}^+ \setminus \Xi\} \times \mathcal{T} \Big| \mathscr{R}e\{f(\mathrm{j}\omega, \boldsymbol{\theta})\} = 0 \text{ and } \mathscr{I}m\{f(\mathrm{j}\omega, \boldsymbol{\theta})\} = 0 \Big\} \tag{4}$$

A guaranteed and robust solution of this $\mathcal{CSP}$ can be obtained, in the searching domain, using interval arithmetics introduced in the next section.

3.1 Basic tools of interval arithmetics

Interval analysis was initially introduced by Moore Moore (1966). An interval $[a] = [\underline{a}, \overline{a}]$ is a closed, bounded, and connected set of real numbers. The set of all intervals is denoted by $\mathbb{IR}$. Real operations are extended to intervals as follows. Given $[a] \in \mathbb{IR}$ and $[b] \in \mathbb{IR}$:

$$[a] + [b] = [\underline{a} + \underline{b}, \overline{a} + \overline{b}], \tag{5}$$

$$[a] - [b] = [\underline{a} - \overline{b}, \overline{a} - \underline{b}], \tag{6}$$

$$[a] \times [b] = [\min(\underline{ab}, \underline{a}\overline{b}, \overline{a}\underline{b}, \overline{a}\overline{b}), \max(\underline{ab}, \underline{a}\overline{b}, \overline{a}\underline{b}, \overline{a}\overline{b})] \tag{7}$$

$$[a]/[b] = \begin{cases} [a] \times \left[\frac{1}{\overline{b}}, \frac{1}{\underline{b}}\right], & \text{if } 0 \notin [b] \\ (-\infty, \infty), & \text{if } 0 \in [b]. \end{cases} \tag{8}$$

An interval vector (or a box) $[\mathbf{a}]$ of $\mathbb{IR}^n$ is a cartesian product of n intervals $[a_i]$ for $i = 1, \ldots, n$.

Additionally, arithmetic operations on intervals often introduce pessimism because the result of each operation must be included in an interval. Considering $g : \mathbb{R}^n \to \mathbb{C}$, a function denoted $[g]$, is an inclusion function of g, if and only if:

$$\forall [\mathbf{x}] \in \mathbb{IR}, g([\mathbf{x}]) \subseteq [g]([\mathbf{x}]) \tag{9}$$

An inclusion function of g is obtained by replacing each standard function of elementary functions by an interval evaluation. In practice, the inclusion function is not unique.

Complex interval analysis

In this paper, complex-valued characteristic functions are considered. Evaluating such functions requires defining complex interval representations. Three kinds of complex representations exist Candau, Raissi, Ramdani & Ibos (2006): rectangular, circular and sectorial. Unfortunately, none of these representations is closed with respect to the arithmetic operations $\{+, -, \times, /\}$. All along the paper, the rectangular representation is used or equivalently real intervals applied on real and imaginary parts of the characteristic function.

3.2 Solving the $\mathcal{CSP}$

The characterization of the whole solution set $\mathbb{S}$ in (4) can be formulated as a set inversion problem

$$\mathbb{S} = f^{-1}(0) \cap \left\{\mathbb{R}^+ \setminus \Xi\right\} \times \mathcal{T} \tag{10}$$

and solved by guaranteed methods based on contraction and bisection.

3.2.1 Contractors

The $\mathcal{CSP}$ (3) can be solved by a contractor $\mathcal{C}$, which is an operator which permits to reduce the domain

$$[\boldsymbol{\zeta}] = ([\omega], [\boldsymbol{\theta}]) \tag{11}$$

without any bisection. Hence, contracting the box $[\boldsymbol{\zeta}]$ means replacing it by a smaller box $[\boldsymbol{\zeta}]^*$ such that the solution set $\mathbb{S}$ remains unchanged, i.e. $\mathbb{S} \subset [\boldsymbol{\zeta}]^* \subset [\boldsymbol{\zeta}]$ Jaulin, Kieffer, Didrit & Walter (2001). There exists different types of contractors depending on whether the system to be solved is linear or not.

The contractor presented in the sequel is based on Waltz filtering algorithm Waltz (1975), extended in Davis (1987); Cleary (1987) to deal with intervals. The main idea is to split a principal constraint into elementary ones. Each elementary constraint involves primitive operators and functions. The next example illustrates how a given constraint is used to contract a domain.

Example Consider

$$\begin{cases} f(\mathbf{a}) = a_3 - a_2 a_1 = 0, \\ a_1 \in [2, 10],\ a_2 \in [1, 10],\ a_3 \in [1, 5]. \end{cases} \tag{12}$$

This problem can also be written as

$$a_3 = a_2 a_1.$$

Applying a forward constraint propagation allows to remove all values from $[a_3]$ that are inconsistant

$$[a_3] = ([a_1] \times [a_2]) \cap [a_3] = [2, 5].$$

The backward constraint propagation allows to remove values from a_1 and a_2 that are inconsistant

$$[a_1] = ([a_3]/[a_2]) \cap [a_1] = [2, 5],$$

$$[a_2] = ([a_3]/[a_1]) \cap [a_2] = [1, 5/2].$$

As a result, following forward and backward propagation, the obtained contracted box that contains the solution is $[\mathbf{a}] = \left([2, 5], [1, 5/2], [2, 5]\right)^T$.

However, sometimes contractors are not capable of reducing enough the parametric domain. Bisection of the variable vector $[\mathbf{a}]$ is then necessary.

```
1: procedure SIVIA(in: [t], [ζ], η, S̄ ; out: S̄)
2:     option: call contractor (in: [ζ] ; out [ζ])
3:     if [t]([ζ]) = [0] then return;
4:     end if
5:     if w([ζ]) ≤ η then
6:         S̄ := S̄ ∪ [ζ];
7:         return;
8:     else
9:         bisect [ζ] into [ζ1] and [ζ2];
10:        S̄ = SIVIA ([t] , [ζ1], η, S̄)
11:        S̄ = SIVIA ([t] , [ζ2], η, S̄)
12:        return;
13:    end if
14: end procedure
```

Algorithm 1. SIVIA algorithm with only an outer enclosure

3.3 Set Inversion Via Interval Analysis (SIVIA)

The SIVIA algorithm Jaulin & Walter (1993) has been proposed to solve constraint propagation problems using bisection. It has been used in different contexts such as: state and parameter estimation for non linear systems Raissi, Ramdani & Candau (2004), robust estimation of frequency domain models Khemane, Malti, Raissi & Moreau (2012), parameter estimation in a glucose model Herrero, Delaunay, Jaulin, Georgiou, Oliver & Toumazou (2016), or even to compute invariant sets of closed-loop control systems Romig, Jaulin & Rauh (2019).

Applying the SIVIA algorithm to (3) allows obtaining an outer $\overline{\mathbb{S}}$ enclosure of the solution set $\mathbb{S}$, if it exists [2] as defined in (4), such that

$$\mathbb{S} \subseteq \overline{\mathbb{S}}. \tag{13}$$

SIVIA is a recursive algorithm based on partitioning of the parameter set into three regions: feasible, indeterminate and unfeasible. From (13), only indeterminate and unfeasible regions (as indicated in the footnote 2) may be obtained. Hence the presentation of the SIVIA algorithm is restrained to these two cases. SIVIA uses an inclusion test $[t] : \{\mathbb{R}^+ \setminus \Xi\} \times \mathcal{T} \to \mathbb{N}$ which is a function allowing to prove if a box $[\boldsymbol{\zeta}]$ is unfeasible or undetermined. If unfeasible, the box is simply ignored. If undetermined, it is bisected and tested again unless its width $w([\boldsymbol{\zeta}])$ is less than a precision parameter η tuned by the user and which ensures that the algorithm terminates after a finite number of iterations.

The outer enclosure $\overline{\mathbb{S}}$ is then computed as a union of

[2] The original SIVIA algorithm allows computing additionally an inner enclosures: $\underline{\mathbb{S}} \subseteq \mathbb{S} \subseteq \overline{\mathbb{S}}$. However, the $\mathcal{CSP}$ formulated in (3), can only yield an outer enclosure $\overline{\mathbb{S}}$. Hence, the presentation of the SIVIA algorithm is restrained to evaluating $\overline{\mathbb{S}}$.

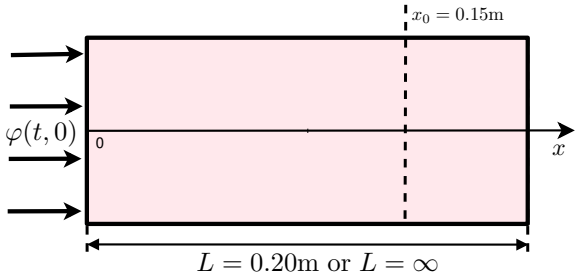

Fig. 3. Thin rod of length L.

all undetermined boxes as indicated in line 6 of Algorithm 1. Line 2 allows calling optionally a contractor at each execution of the SIVIA algorithm. The complexity of the SIVIA algorithm is exponential with respect to the number of parameters. The SIVIA algorithm is implemented using INTLAB toolbox Rump (1999) in different contexts: a controlled heat equation in section 4, rational TDSs in section 5, and fractional systems is section 6.

4 Application to stability analysis of a distributed parameter system

Consider a one-dimensional heat diffusion in a thin rod [3] of length $0 < L \leq \infty$. The rod is thermally isolated, except at its boundary cross-sections as in Fig.3.

At the initial end $x = 0$, the rod is subject to an adjustable thermal flux, $\varphi(t,0) = -\lambda \frac{\partial \theta}{\partial x}(t,0)$, where λ is the thermal conductivity. Two cases are treated: either the rod is of finite length or infinite. When the rod length is finite, the opposite end is kept at ambient temperature $\theta(t,L) = 0$. The corresponding model describing spatio-temporal distribution of the temperature along the rod is given by the well-known *heat equation*,

$$\frac{\partial^2 \theta(t,x)}{\partial x^2} = \sigma^{-1} \frac{\partial \theta(t,x)}{\partial t} \,, \tag{14}$$

where σ is the thermal diffusivity of the medium.

The temperature of the rod is measured at a cross-section $x = x_0 = 0.15$m, with $0 \leq x_0 \leq L$. This temperature is then controlled remotely (see Fig.4) using a proportional controller with a gain K. Additionally, time required to transmit data from the controller to the actuator, and from the sensor to the controller is denoted by $\frac{\tau}{2}$, so that the total loop delay is $\tau \geq 0$. Hence, the effective transfer function of the proportional delayed controller is

$$P(s) = K e^{-\tau s} \tag{15}$$

[3] For numerical application, the rod is considered of aluminium type with a thermal diffusivity $\sigma = 98.8 \times 10^{-6}$ m^2/s and a conductivity $\lambda = 237$ Wm^{-1}K^{-1} (see e.g. Baehr & K. (2011)).

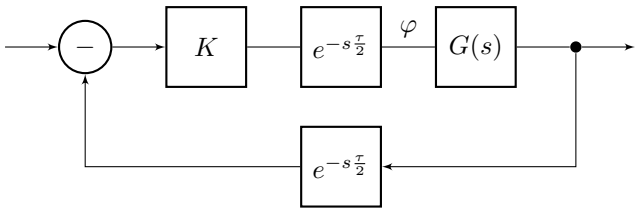

Fig. 4. A feedback control loop, where $G(s)$ is the transfer function between the heat flux and the temperature at x_0, for either a semi-infinite or a finite rod, $P(s)$ is a proportional delayed controller as in (15).

The objective of this example is to find the whole set of stabilizing controllers (15) in the K versus τ plane in both cases: finite and semi-infinite rods. A similar problem is treated in Morărescu & Niculescu (2007), with the same delayed proportional controller $P(s)$, however applied to a rational system.

4.1 Semi-infinite spatial domain ($L = \infty$)

In the semi-infinite domain, the transfer function between the input flux and the temperature at the selected cross-section is Curtain & Morris (2009)

$$G(s) = \frac{\Theta(s,x)}{\Phi(s,0)} = \frac{e^{-x\sqrt{\frac{s}{\sigma}}}}{\lambda\sqrt{\frac{s}{\sigma}}} \,, \tag{16}$$

giving rise to the following closed-loop transfer function,

$$\frac{P(s)G(s)}{1 + P(s)G(s)} = \frac{K e^{-s\tau} e^{-x\sqrt{\frac{s}{\sigma}}}}{\lambda\sqrt{\frac{s}{\sigma}} + K e^{-s\tau} e^{-x\sqrt{\frac{s}{\sigma}}}} \,, \tag{17}$$

and the following closed-loop characteristic function

$$f(s,K,\tau) = \lambda\sqrt{\frac{s}{\sigma}} + K e^{-s\tau} e^{-x\sqrt{\frac{s}{\sigma}}} \,. \tag{18}$$

Due to the presence of $\sqrt{s}$, a branch-cut is necessary. It is chosen along the negative real axis including the branching point 0 and ∞. Hence, the characteristic function $f(s,K,\tau)$ is holomorphic in the complement of the branch-cut line of the complex plane and the arguments of s are restrained to

$$|\arg(s)| < \pi \tag{19}$$

Root continuity of $f(s,K,0)$

In the special case when $\tau = 0$, all the roots of $f(s,K,0)$ can be determined analytically and their locus plotted versus K. The roots of $f(s,K,0)$ satisfy

$$x\sqrt{\frac{s}{\sigma}} e^{x\sqrt{\frac{s}{\sigma}}} = -\frac{Kx}{\lambda} \tag{20}$$

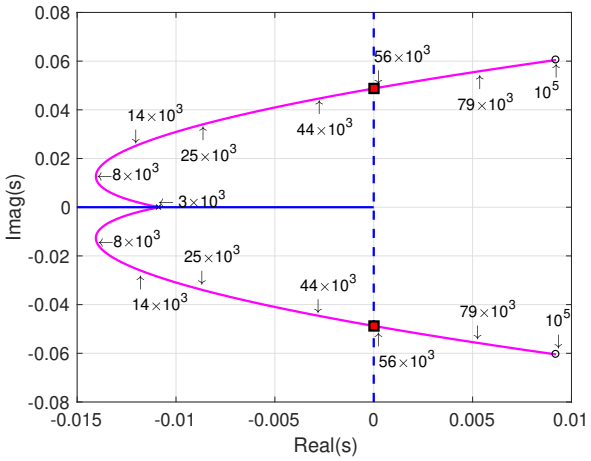

Fig. 5. Root locus of $f(s, K, 0)$ in (18) for different values of K, illustrating that poles pop up from the plane-cut. When the poles cross the imaginary axis (red squares), the system becomes unstable. Numbers on the curves correspond to values of K. The plane-cut is represented in blue along $\mathbb{R}^-$.

provided (19) is fulfilled. The solutions of (20) are given by all the determinations, $n = 0, \pm 1, \pm 2, \ldots$, of Lambert's W_n function, see e.g. Corless, Gonnet, Hare, Jeffrey & Knuth (1996),

$$x\sqrt{\frac{s}{\sigma}} = W_n\left(-\frac{Kx}{\lambda}\right), \tag{21}$$

provided, (19) is fulfilled, i.e. provided

$$\left|\arg\left(\sqrt{s}\right)\right| = \left|\arg\left(W_n\left(-\frac{Kx}{\lambda}\right)\right)\right| < \frac{\pi}{2} \tag{22}$$

Hence, all the solutions

$$s = \frac{\sigma}{x^2} W_n^2\left(-\frac{Kx}{\lambda}\right), \quad n = 0, \pm 1, \pm 2, \ldots \tag{23}$$

constrained by (22), are roots of the characteristic function $f(s, K, 0)$. The root locus of $f(s, K, 0)$ is plotted versus gain K, in Fig.5, for the principal determination of the Lambert function W_0 (as upper imaginary part) and for the determination W_{-1} (as lower imaginary part). The other determinations of $W_n, n = 1, \pm 2, \pm 3, \ldots$ are not represented as they are well beyond the scale of Fig.5 towards $-\infty$. They may yield other poles crossing the imaginary axis for values of K that are much greater than the ones represented in Fig.5, which shows that two poles stem from the branch-cut when $K \approx 3 \times 10^3$. They cross the imaginary axis towards instability when $K \approx 56 \times 10^3$. The objective of the paper is to determine for what parametric values (here K and in a more general case K and τ) the poles cross the imaginary axis.

4.2 Finite spatial domain ($L < \infty$)

In this case, the following transfer function is obtain for the heat diffusion process under consideration Curtain & Morris (2009)

$$G(s) = \frac{\Theta(s, x)}{\Phi(0, s)} = \frac{\sinh((L - x)\sqrt{\frac{s}{\sigma}})}{\lambda\sqrt{\frac{s}{\sigma}}\cosh(L\sqrt{\frac{s}{\sigma}})}, \tag{24}$$

giving rise to the following closed-loop transfer function

$$\frac{P(s)G(s)}{1 + P(s)G(s)} = \frac{Ke^{-s\tau}\sinh\left((L - x)\sqrt{\frac{s}{\sigma}}\right)}{\lambda\sqrt{\frac{s}{\sigma}}\cosh\left(L\sqrt{\frac{s}{\sigma}}\right) + Ke^{-s\tau}\sinh\left((L - x)\sqrt{\frac{s}{\sigma}}\right)}. \tag{25}$$

Its stability is assessed in the parametric space K versus τ by applying the proposed algorithm to the following characteristic function

$$f(s, K, \tau) = \lambda\sqrt{\frac{s}{\sigma}}\cosh\left(L\sqrt{\frac{s}{\sigma}}\right) + Ke^{-s\tau}\sinh\left((L - x)\sqrt{\frac{s}{\sigma}}\right). \tag{26}$$

4.3 Robust estimation algorithm of the SCS

Both characteristic functions (18) and (26) comply with the hypotheses (H1)-(H3). They have a branching point at $s = 0$ (hence $\Xi = \{0\}$), which is excluded from the searching box, initialized at

$$[\boldsymbol{\zeta}] = ([\omega], [K], [\tau]) = \left([\varepsilon, 0.1], [0, 7 \cdot 10^4], [0, 100]\right) \tag{27}$$

with $\varepsilon > 0$. Although theoretically the searching interval of ω is $\mathbb{R}^+ \setminus \Xi$, the thermal system under consideration is slow. Additionally, one can see from Fig.5 that the root locus of (18) for $\tau = 0$ crosses the imaginary axis for an ω in the interval $(0.04, 0.05)$. Consequently, the first poles crossing the imaginary axis towards instability, in both cases (18) for any τ and (26), are expected to be within the frequency interval $(0 \quad 0.1]$ rad/sec. In case this initial interval is not wide enough, then the obtained outer enclosures of the interval $[\omega]$ will touch the upper bound 0.1. In this case, the searching interval is enlarged and the SIVIA algorithm run again. The tolerance is set to an arbitrarily small value as the width of each element $w([\boldsymbol{\zeta}])$ divided by 2^8

$$\eta = w([\boldsymbol{\zeta}])/2^8 \tag{28}$$

$$\eta = (0.39 \cdot 10^{-3}, 273.4, 0.39) \tag{29}$$

The obtained outer enclosures of the stability crossing sets is plotted in the K versus τ plane in Fig.6 in red

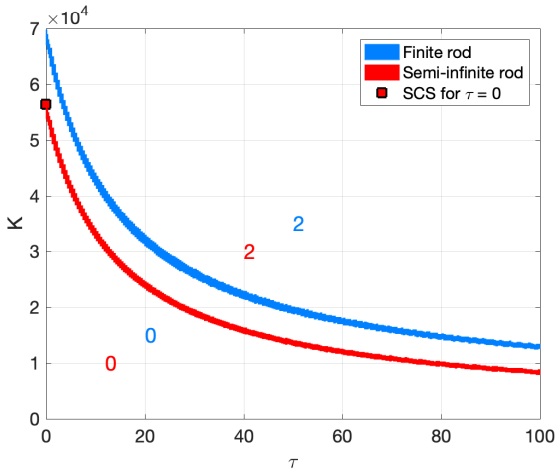

Fig. 6. SCS in the finite and semi-infinite aluminium rods. The number of unstable poles is indicated in each regions (by the corresponding color). The red square corresponds to the SCS of $f(s, K, 0)$ in (18) as predicted in the root locus of Fig.5 (red square).

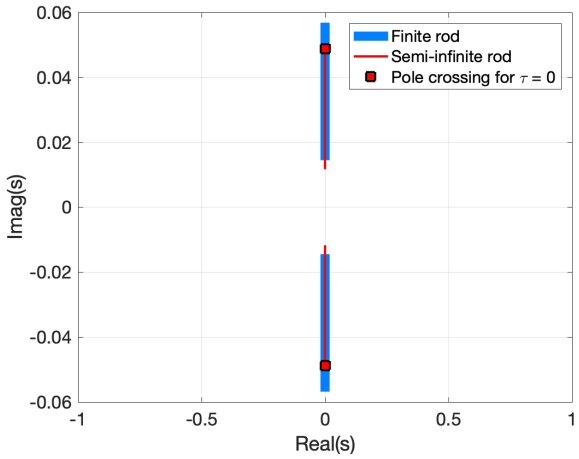

Fig. 7. Poles crossing the imaginary axis in the finite and semi-infinite aluminium rods. The red squares correspond to the pole crossing of $f(s, K, 0)$ in (18) as predicted in the root locus of Fig.5 (red square).

for the semi-infinite rod and in blue for the finite rod. The position of the poles crossing the imaginary axis is plotted, with the same colors, in Fig.7.

The red line (similarly the blue) in Fig.6 splits the plane into two regions: a guaranteed stability region (the lower left containing $K = 0$ and $\tau = 0$) and a guaranteed instability region as the upper right one. In between, the outer enclosures of the SCS are plotted. Their width can be reduced by reducing the precision factor η in (28) at the price of a higher computational burden. In the case of the semi-infinite rod, for $\tau = 0$, the results of Figs.6 and 7 (red squares) are confirmed by the intersection of the root-locus with the imaginary axis, in Fig.5.

To the best of authors' knowledge, in both cases finite with $\tau \neq 0$ and semi-infinite aluminium rods, there is no analytical method allowing to compute the roots of the characteristic function f in (18) or (26). The only alternative method for evaluating stability of the control loop is based on a graphical representation that uses Cauchy's principle argument.

5 Application to stability analysis of time delay systems

5.1 *Distributed delay system*

Consider in this section a distributed delay system taken from (Turkulov et al., 2022, example 9) modeled by

$$\dot{x}(t) = -\int_{-\tau}^{0} e^{K\alpha} x(t+\alpha) d\alpha. \tag{30}$$

Its characteristic function, computed by straightforward integration of the Laplace transform of (30),

$$f(s, K, \tau) = s^2 + sK + 1 - e^{-\tau(s+K)}, \tag{31}$$

complies with the hypotheses (H1)-(H3), with no singularities in $\overline{\mathbb{C}^+}$. Hence the stability is investigated in

$$[\boldsymbol{\zeta}] = ([\omega], [K], [\tau]) = ([0, 1.5], [0, 0.3], [0, 20]), \tag{32}$$

and the tolerance set as in (28).

The obtained outer enclosure of the SCS is plotted in the K versus τ plane in Fig.8. The number of unstable poles, computed at any point inside the different regions, is indicated by a number. Fig.8 confirms the results of (Turkulov et al., 2022, example 8) obtained using Rouché's theorem. The outer enclosure of $[\omega]$, for which the poles cross the imaginary axis, is $[0.31, 1.42]$.

5.2 *Time delay system of retarded-type*

Consider a TDS system of retarded type, taken from (Turkulov et al., 2022, example 10), with a characteristic function given by

$$f(s, \tau_1, \tau_2) = s^2 + 2se^{-s\tau_1} + e^{-s\tau_2}. \tag{33}$$

Its stability is investigated with respect to τ_1 and τ_2 by setting the initial searching box to

$$[\boldsymbol{\zeta}] = ([\omega], [\tau_1], [\tau_2]) = ([0.45, 2.5], [0, 1.8], [0, 3]). \tag{34}$$

The obtained outer enclosure of the SCS is plotted in the τ_1 versus τ_2 plane in Fig.9. The number of unstable poles, computed at any point inside the different regions, is indicated by a number. Fig.9 confirms again the results

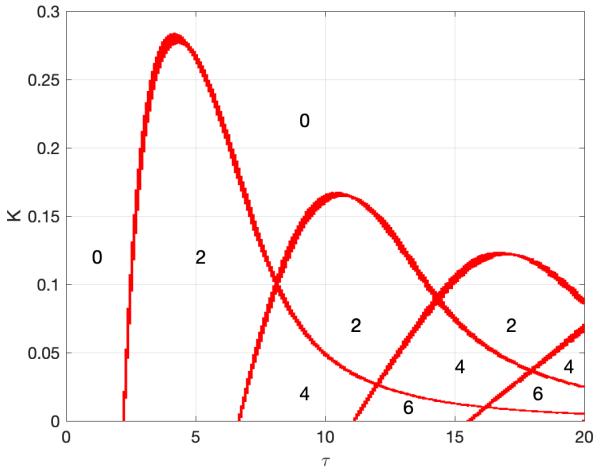

Fig. 8. Stability crossing sets of $f(s, K, \tau)$ in (31) in K versus τ plane and the number of unstable poles in each delimited region. The number of unstable poles is indicated in each region.

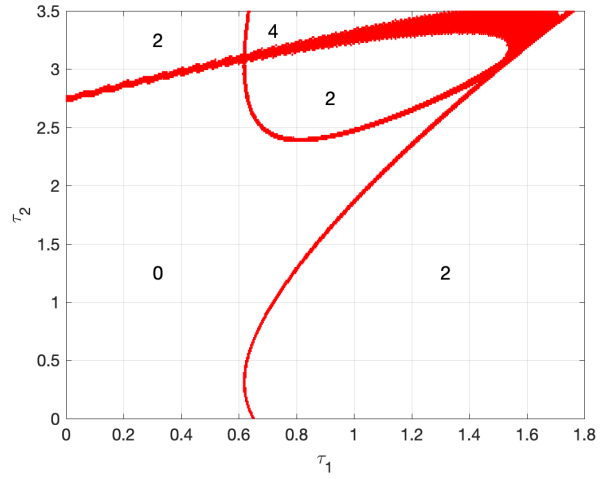

Fig. 9. Stability crossing sets of $f(s, \boldsymbol{\tau})$ in (33) in τ_2 versus τ_1 plane and the number of unstable poles in each delimited region. The number of unstable poles is indicated in each region.

of (Turkulov et al., 2022, example 10) obtained using Rouché's theorem. The obtained outer enclosure of the interval of $[\omega]$ for which the poles cross the imaginary axis is $[0.48, 2.42]$.

6 Application to stability analysis of a fractional system

Consider in this section a fractional system, taken from (Rapaić & Malti, 2019, example 3), which characteristic function is given by

$$f(s, \alpha_1, \alpha_2) = s^{\alpha_2} + 2s^{\alpha_1} + 1 \tag{35}$$

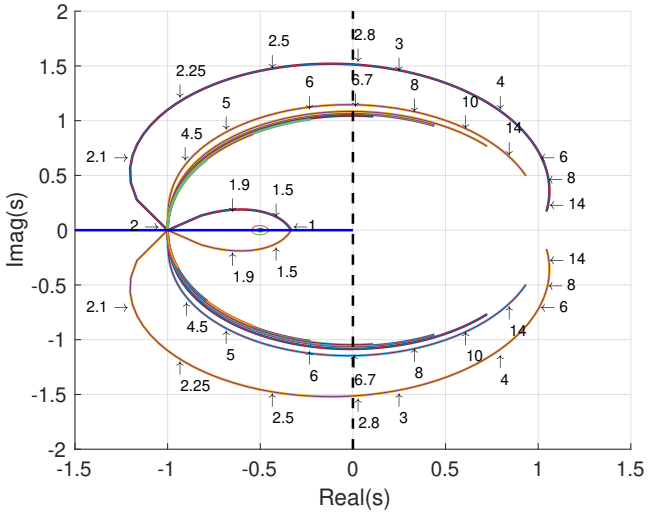

Fig. 10. Root locus of $f(s, 1, \alpha_2)$ versus α_2, illustrating that poles are pop up from and vanish into the plane-cut. Numbers on the two outer most curves correspond to values of α_2. The plane-cut, along $\mathbb{R}^-$, is represented in blue. When the roots cross the imaginary axis the first time (here for $\alpha_2 = 2.8$), the corresponding system becomes unstable.

and $(\alpha_1, \alpha_2) \in \{\mathbb{R}^+ \setminus \{0\}\}^2$.

When α_1 and/or α_2 are non integers, the characteristic function $f(s, \alpha_1, \alpha_2)$ is holomorphic in the complement of the branch-cut line of the complex plane. The branch-cut is chosen to be along the negative real axis including the branching point 0 and ∞, and the restriction (19) applies to s. However, when both α_1 and α_2 are integers, no branch-cut is required and the zeros of f may be located on the negative real axis.

6.1 *Root continuity of* $f(s, 1, \alpha_2)$

Stability can be analyzed by checking the position of the zeros of the characteristic function $f(s, 1, \alpha_2)$, that are in the principal Riemann sheet, i.e. that satisfy (19). The roots of

$$f(s, 1, \alpha_2) = s^{\alpha_2} + 2s^1 + 1 \tag{36}$$

are computed numerically for $0 < \alpha_2 < 20$ with a step of $\delta = \frac{1}{40}$, by finding all the roots of the following polynomial (with the change of variable $p = s^\delta$)

$$f\left(p^{\frac{1}{\delta}}, 1, \alpha_2\right) = p^{\frac{\alpha_2}{\delta}} + p^{\frac{1}{\delta}} + 1\,, \tag{37}$$

that satisfy (19), applied to p, i.e.

$$|\arg(p)| = |\arg(s^\delta)| < \delta\pi. \tag{38}$$

The number of roots, plotted in Figs.10 and 11, depends on the value of α_2. When

- $0 < \alpha_2 < 1$, $f(s, 1, \alpha_2)$ has no root,

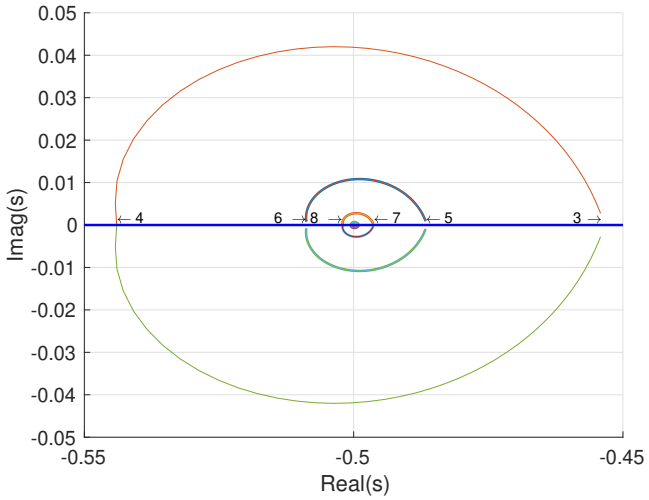

Fig. 11. A zoom of Fig.10 around $(\mathscr{Im}(s), \mathscr{Re}(s)) = (0, -0.5)$, showing that new poles pop up from the plane-cut when $\alpha_2 = 3, 5, 7, \ldots$ and vanish into the plane-cut when α_2 gets bigger than $4, 6, 8, \ldots$

- $\alpha_2 = 1$, a simple root appears at $s = -\frac{1}{3}$,
- α_2 gets slightly bigger than 1, the root at $s = -\frac{1}{3}$ splits into two complex conjugate roots,
- $\alpha_2 = 2$, the two complex conjugate roots merge into a real root of multiplicity 2 at $s = -1$,
- α_2 gets bigger than 2, the double root splits into two complex-conjugate ones which move along the outer most curve of Fig.10,
- $\alpha_2 \approx 2.8$, the roots cross the imaginary axis, and the corresponding system becomes unstable,
- $\alpha_2 = 3$, the sequence of two complex conjugate roots continues evolving in the right-half complex plane and a new root is created at $s \approx -0.455$ (see Fig.11),
- α_2 gets bigger than 3, the real root splits into two complex-conjugate ones,
- $\alpha_2 = 4$ the two complex conjugate roots merge again into a simple root at $s \approx -0.543$ and a new root is created at $s = -1$,
- α_2 gets bigger that 4, the simple root at $s \approx -0.543$ vanishes into the plane-cut and the one at $s = -1$ splits into two complex conjugate roots yielding the sequence plotted as the second outer most curve in Fig.10.
- $\alpha_2 \approx 6.7$, two more complex conjugate roots cross the imaginary axis.
- ... and so on.

All in all, roots pop up from and vanish into the plane-cut. The number of roots crossing the imaginary axis affect system stability. Again, the objective of this example is to determine for what parametric values (here α_1 and α_2) the poles cross the imaginary axis.

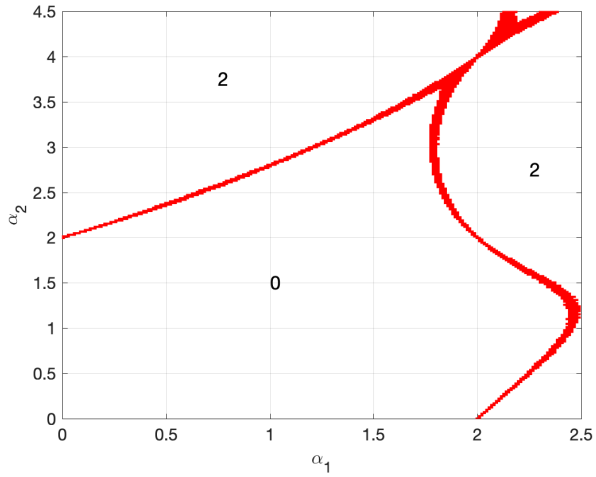

Fig. 12. Stability crossing sets of $f(s, \alpha_1, \alpha_2)$ in (33) in α_2 versus α_1 plane. The number of unstable poles is indicated in each delimited region. Along the vertical axis $\alpha_1 = 1$, the stability limit corresponds to $\alpha_2 \approx 2.8$ as predicted in the root locus of Fig.10.

6.2 Robust estimation algorithm of the SCS

In this subsection, the proposed algorithm is applied for determining the SCS of $f(s, \alpha_1, \alpha_2)$ in (35). The characteristic function (35) complies with the hypotheses (H1)-(H3). It has a branching point at $s = 0$ (hence $\Xi = \{0\}$), which is excluded from the searching box. Two initializations are considered. The first one aims at establishing the stability region in the parametric space

$$[\boldsymbol{\zeta}] = ([\omega], [\alpha_1], [\alpha_2]) = ([\varepsilon, 4], [\varepsilon, 3], [\varepsilon, 4.5]) \qquad (39)$$

with $\varepsilon > 0$. The second one allows establishing wider regions in the parametric space having the same number of unstable poles

$$[\boldsymbol{\zeta}] = ([\omega], [\alpha_1], [\alpha_2]) = ([\varepsilon, 4], [\varepsilon, 15], [\varepsilon, 20]) \qquad (40)$$

In both cases the tolerance is set to (28).

The obtained outer enclosures $\overline{\mathbb{S}}$ of the SCS, are plotted in Fig.12 for the first initialization (39) and in Fig.13 for the second initialization (40). Fig.12 confirms the results of (Rapaić & Malti, 2019, example 3), obtained using Rouché's theorem. The outer enclosures of the interval $[\omega]$ for which the poles cross the imaginary axis are respectively $[0.56, 1.75]$ and $[0.56, 1.79]$.

It can easily be verified, along the vertical axis $\alpha_1 = 1$, that the stability limit corresponds to $\alpha_2 \approx 2.8$ as predicted in the root locus of Fig.10, which also confirms the validity of the results, when $\alpha_1 = 1$. Hence, all fractional systems, incommensurate and commensurate, that have differentiation orders in the lower-left region of Fig.12, have no unstable pole.

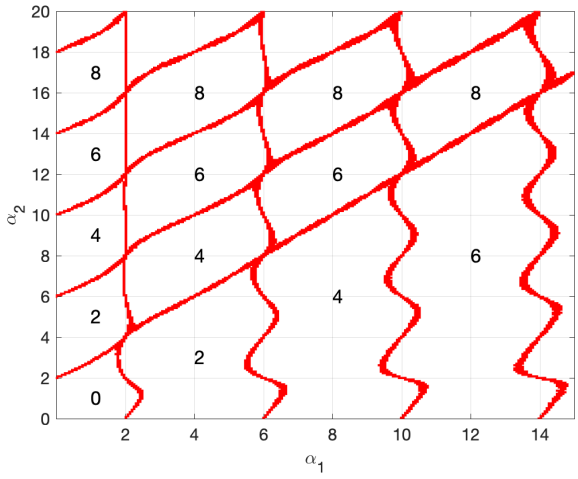

Fig. 13. Stability Crossing Sets (wider interval search as compared to Fig.12). The number of unstable poles is indicated in each region. Along the vertical axis $\alpha_1 = 1$, the next crossing appears at $\alpha_2 \approx 6.7$, as predicted in the root locus plot in Fig.10.

7 Conclusions

A unified framework has been presented in this paper for stability analysis of irrational transfer functions in the frequency domain, under some mild hypotheses. First, it has been proven that the only way for the number of zeros of a characteristic function (transfer function poles) in the right-half complex plane, to change, when its parameters vary continuously, is by crossing the imaginary axis. Based on this theoretical result, the problem of finding the set of parameters for which poles cross the imaginary axis (Stability Crossing Sets (SCS)), is formulated as a constraint satisfaction problem. It is solved using the robust SIVIA algorithm, based on interval arithmetics, that uses contraction and bissection. The developed algorithm has successfully been used for determining the SCS of (i) a controlled parabolic 1D partial differential equation, namely the heat equation, in finite and semi-infinite media, (ii) time-delay rational systems with distributed and retarded type delays, (iii) fractional systems, providing stability results even for incommensurate differentiation orders. The proposed algorithm may be used for any number of transfer function parameters. The only limitation is related to the time-complexity of the SIVIA algorithm which is known to be exponential in terms of the number of parameters. The examples presented in the paper have been intentionally limited to two parameters for graphical representation purpose.

References

Aghayan, Z. S., Alfi, A., & Machado, J. T. (2021). Robust stability of uncertain fractional order systems of neutral type with distributed delays and control input saturation. *ISA Transactions*, *111*, 144–155.

Baehr, H. D. & K., S. (2011). *Heat and Mass Transfer* (3rd ed.). Springer.

Candau, Y., Raissi, R., Ramdani, N., & Ibos, L. (2006). Complex interval arithmetic using polar form. *Reliable Computing*, *12*(1), 1–20.

Chait, Y., MacCluer, C., & Radcliffe, C. (1989). A nyquist stability criterion for distributed parameter systems. *IEEE Transactions on Automatic Control*, *34*(1), 90–92.

Cleary, J. C. (1987). Logical arithmetic. *Future Computing Systems*, *2*(2), 125–149.

Cooke, K. L. & Grossman, Z. (1982). Discrete delay, distributed delay and stability switches. *Journal of Mathematical Analysis and Applications*, *86*(2), 592 – 627.

Corless, R. M., Gonnet, G. H., Hare, D. E. G., Jeffrey, D. J., & Knuth, D. E. (1996). On the lambertw function. *Advances in Computational Mathematics*, *5*(1), 329–359.

Curtain, R. & Morris, K. (2009). Transfer functions of distributed parameter systems: A tutorial. *Automatica*, *45*(5), 1101–1116.

Davis, E. (1987). Constraint propagation with interval labels. *Artificial Intelligence*, *32*(3), 281–331.

Dieudonné, J. (1960). *Foundations of Modern Analysis*. Academic Process, NY and London.

El'sgol'ts, L. E. & Norkin, S. B. (1973). *Introduction to the Theory and Application of Differential Equations with Deviating Arguments*. Academic Press, Inc. (London) LTD.

Fridman, E. & Orlov, Y. (2009). Exponential stability of linear distributed parameter systems with time-varying delays. *Automatica*, *45*(1), 194–201.

Gao, R., Ma, N., & Sun, G. (2019). Stability of solution for uncertain wave equation. *Applied Mathematics and Computation*, *356*, 469–478.

Gryazina, E. (2004). The D-decomposition theory. *Automation and Remote Control*, *65*, 1872–1884.

Gu, K. & Naghnaeian, M. (2011). Stability crossing set for systems with three delays. *IEEE Transactions on Automatic Control*, *56*(1), 11–26.

Gu, K., Niculescu, S.-I., & Chen, J. (2005). On stability crossing curves for general systems with two delays. *Journal of Mathematical Analysis and Applications*, *311*(1), 231 – 253.

Ha-Duong, T. & Joly, P. (1994). On the stability analysis of boundary conditions for the wave equation by energy methods. part i: The homogeneous case. *Mathematics of Computation - Math. Comput.*, *62*, 539–563.

Hale, J. & Huang, W. (1993). Global geometry of the stable regions for two delay differential equations. *Journal of Mathematical Analysis and Applications*, *178*(2), 344 – 362.

Herrero, P., Delaunay, B., Jaulin, L., Georgiou, P., Oliver, N., & Toumazou, C. (2016). Robust set-membership parameter estimation of the glucose minimal model. *Int. J. of adaptive control and signal processing*, *30*(2), 173–185.

Ivanova, E., Moreau, X., & Malti, R. (2016). Stability

and resonance conditions of second-order fractional systems. *Journal of Vibration and Control*, 1–15.

Jaulin, L., Kieffer, M., Didrit, O., & Walter, E. (2001). *Applied interval analysis*. London: Springer-Verlag.

Jaulin, L. & Walter, E. (1993). Set inversion via interval analysis for nonlinear bounded-error estimation. *Automatica*, *29*(4), 1053–1064.

Katz, R. & Fridman, E. (2020). Constructive method for finite-dimensional observer-based control of 1-d parabolic pdes. *Automatica*, *122*, 109285.

Katz, R. & Fridman, E. (2021). Delayed finite-dimensional observer-based control of 1-d parabolic pdes. *Automatica*, *123*, 109364.

Khemane, F., Malti, R., Raissi, T., & Moreau, X. (2012). Robust estimation of fractional models in the frequency domain using set membership methods. *Signal Processing*, *92*, 1591–1601.

Lee, M. S. & Hsu, C. S. (1969). On the tau-decomposition method of stability analysis for retarded dynamical systems. *SIAM Journal on Control*, *7*(2), 242–259.

Lhachemi, H., Saussié, D., Zhu, G., & Shorten, R. (2020). Input-to-state stability of a clamped-free damped string in the presence of distributed and boundary disturbances. *IEEE Transactions on Automatic Control*, *65*(3), 1248–1255.

Li, L. & Gao, H. (2021). The stability and stabilization of heat equation in non-cylindrical domain. *Journal of Mathematical Analysis and Applications*, *493*(2), 124538.

Li, L., Zhou, X., & Gao, H. (2018). The stability and exponential stabilization of the heat equation with memory. *Journal of Mathematical Analysis and Applications*, *466*(1), 199–214.

Logemann, H. (1991). Circle criteria, small-gain conditions and internal stability for infinite-dimensional systems. *Automatica*, *27*(4), 677–690.

Moore, R. (1966). *Interval analysis*. Englewood Cliffs, NJ: Prentice-Hall.

Morărescu, C.-I. & Niculescu, S. (2007). Stability crossing curves of SISO systems controlled by delayed output feedback. *Dynamics of Continuous, Discrete and Impulsive Systems Series B: Applications & Algorithms*, *14*, 659–678.

Morărescu, C.-I., Niculescu, S.-I., & Gu, K. (2007). Stability crossing curves of shifted gamma-distributed delay systems. *SIAM Journal on Applied Dynamical Systems*, *6*(2), 475–493.

Neimark, Y. I. (1998). D-partition and robust stability. *Computational Mathematics and Modeling*, *9*(2), 160–166.

Prieur, C. & Trélat, E. (2019). Feedback stabilization of a 1-d linear reaction–diffusion equation with delay boundary control. *IEEE Transactions on Automatic Control*, *64*(4), 1415–1425.

Raissi, T., Ramdani, N., & Candau, Y. (2004). Set membership state and parameter estimation for systems described by nonlinear differential equations. *Automatica*, *40*(10), 1771–1777.

Rapaić, M. R. & Malti, R. (2019). On stability regions of fractional systems in the space of perturbed orders. *IET Control Theory & Applications*, *13*.

Romig, S., Jaulin, L., & Rauh, A. (2019). Using interval analysis to compute the invariant set of a nonlinear closed-loop control system. *Algorithms*, *12*(12).

Rump, S. (1999). *Developments in reliable computing*, chapter IntLab – Interval laboratory, (pp. 77–104). Kluwer academic publisher.

Sano, H. (2018). Stability analysis of the telegrapher's equations with dynamic boundary condition. *Systems & Control Letters*, *111*, 34–39.

Sipahi, R. & Delice, I. I. (2009). Extraction of 3D stability switching hypersurfaces of a time delay system with multiple fixed delays. *Automatica*, *45*(6), 1449 – 1454.

Sipahi, R. & Olgac, N. (2005). Complete stability robustness of third-order LTI multiple time-delay systems. *Automatica*, *41*(8), 1413 – 1422.

Turkulov, V., Rapaić, M. R., & Malti, R. (2022). Stability analysis of time-delay systems in the parametric space. *Automatica*. Submitted (see also https://arxiv.org/abs/2103.15629).

Waltz, D. L. (1975). *The psychology of computer vision*, chapter Generating semantic descriptions from drawing of scenes with shadows, (pp. 19–91). New-York: McGraw-Hill, New York.

Zhang, S., Liu, L., & Xue, D. (2020). Nyquist-based stability analysis of non-commensurate fractional-order delay systems. *Applied Mathematics and Computation*, *377*, 125111.